AIMS Materials Science, 3(3): 1208-1221.
DOI: 10.3934/matersci.2016.3.1208
Received: 11 April 2016
Accepted: 30 May 2016
Published: 17 August 2016

http://www.aimspress.com/journal/Materials

Review

On the dynamic compared to static grain growth rate in 3 mole% yttria-stabilized tetragonal zirconia polycrystals (3 Y-TZP)

Jun Wang [1],* and Hans Conrad [2]

[1] Materials Science and Engineering Dept., Rutgers, the State University of New Jersey, Piscataway, NJ 08855-0909, USA
[2] Material Science and Engineering Dept., North Carolina State University Raleigh, NC 27695-7907, USA

* **Correspondence**: Email: jw931@scarletmail.rutgers.edu.

Abstract: The reason for the higher dynamic grain growth rate compared to static rate is considered with focus on the results by Nied and Wadsworth on 3 mole% yttria-stabilized zirconia (3 Y-TZP). Included is a review of the models and theories of the pertinent grain growth kinetics and on the concurrent grain boundary cavitation. It is concluded that the same physical mechanism governs both dynamic and static grain growth, and that the existing grain size is an important factor in both cases. It is further concluded that the major factor responsible for the higher dynamic grain growth rate is the pre-exponential in the Arrhenius-type grain growth kinetics equation, the entropy corresponding to the atomic diffusion being an important parameter. There exists insufficient information to ascertain the influence of grain boundary cavitation on the concurrent dynamic grain growth.

Keywords: zirconia; grain growth; grain size; cavitation; kinetics; entropy

1. Introduction

It is well-known that the mean grain size and the corresponding grain shape and grain size distribution have a significant influence on the processing (e.g., sintering, annealing and forming) of polycrystalline metals and ceramics [1]. Further, it is well-established [2,3] that concurrent grain growth occurs during the plastic deformation of fine-grained materials ("dynamic" grain growth), and that the corresponding dynamic grain growth rate is appreciably greater than that which occurs

during conventional annealing without an applied stress ("static" grain growth). Our understanding of the reason for the greater dynamic grain growth rate compared to static is still incomplete.

It is well-established that the plastic deformation of fine-grained materials generally occurs by grain boundary (GB) sliding [4]. Two physical mechanisms have been proposed for the greater dynamic grain growth due to the GB sliding; see [5,6]: (a) the sliding creates excess vacancies, which leads to an enhancement of the GB mobility and (b) in materials which contain solutes segregated at the GBs the sliding disrupts the segregated solute clusters which normally retard grain growth. Specific, quantitative details regarding the manner in which these models enhance the grain growth rate are however lacking.

A significant paper comparing dynamic and static grain growth rates in ceramics is that by Nich and Wadworth (N-W) [2] on 3 mole% yttria-stabilized zirconia (3Y-TZP) at 1550 ℃ and 1650 ℃. They found that both the dynamic and static grain size obeyed the cubic time law, but that both the activation energy Q (520 vs 580 kJ/mole) and the pre-exponential A (~7.5×10^{10} vs ~10^{12} m/s) were lower for dynamic compared to static grain growth. They attributed the larger dynamic grain growth to an enhancement by the applied stress of atom migration across the GBs. However, no specific or quantitative details are given regarding the manner in which the stress enhances atom migration across the GBs.

To provide additional insight into the physical mechanism(s) by which GB sliding enhances the dynamic grain growth rate, we analyze the data by N-H [2] (and related results) employing a different approach than that used by these authors.

2. Pertinent Models and Physical Mechanisms

2.1. Static grain growth

Theoretical considerations [7–11] give that the mean grain growth rate $\dot{d}$ in polycrystals is the product of the driving force P and the GB mobility M, i.e.,

$$\dot{d} = \mathrm{PM} \tag{1}$$

In pure, unalloyed, and fully-annealed materials,

$$P \cong 2\gamma_b/r \tag{2}$$

where P is the capillary driving force, γ_b is the GB energy, r = (3/2) $\bar{d}$ [12] is the local GB radius of curvature and $\bar{d}$ is the mean linear intercept grain size. The GB mobility is given by

$$\mathrm{M} = \mathrm{M}_0 \exp(-\Delta G^*/\mathrm{kT}) \tag{3}$$

where $\Delta G^* = \Delta H^* - \mathrm{T}\Delta S^*$ is the Gibbs free energy for an atomic jump across the GB to its nearest neighbor, and

$$\mathrm{M}_0 = \mathrm{N_j}\nu x^* \tag{4}$$

where $\mathrm{N_j} \approx \mathrm{A_b}/\Omega^{2/3}$ is the number of atomic sites per unit volume from which an atom (or ion) can jump from one grain onto its neighbor, $\mathrm{A_b} = 2/\bar{d}$ [13,14] is the existing GB area per unit volume

and Ω is the atomic volume, ν is the atomic vibration frequency (Debye frequency) and x* $\approx \Omega^{1/3}$ is the jump distance. Combining Eqs.1–4 one obtains for the static grain growth rate in pure, fully-annealed, single phase materials

$$\dot{d} = \left[\frac{A\gamma_b}{d^2\Omega^{1/3}} \exp\left(\Delta S^*/R\right)\right] \exp\left(-Q/RT\right) \tag{5}$$

where R is the gas constant and $Q \equiv \Delta H^*$. To be noted regarding Eq.5 is that the existing grain size d has *two* effects on the concurrent grain growth rate: (a) on the magnitude of the driving force P and (b) on the number of sites available for atomic jumps from one grain to the next. The latter effect has generally been neglected in considerations of grain growth. It accounts for the cubic grain growth time law being generally observed, rather than a square time law.

The relationship for static grain growth rate in impure materials or those which contain solute additions is more complex than Eq.5. This is due to the segregation of the impurity or solute ions at the GBs, which thereby exert a drag on the GB mobility [8,9], and is generally referred to as Cahn's solute drag theory. Vandermeer [15] has pointed out that according to Cahn's solute drag theory the grain growth rate vs the driving force behavior is that shown in Figure1. The slope of the log$\dot{d}$ vs log P curve shown is unity at low (Regime I) and high (Regime III) values of the driving force, and appreciably larger in the transition (Regime II). Further, according to Vandermeer [15], the rate controlling mechanism in Regime I is the diffusion of solute atoms (or ions) perpendicular to the GB and that in Region III by the solvent atoms (ions) across the boundary. As pointed out by Cahn [8] any activation energy determined from the temperature dependence of $\dot{d}$ in the transition regime has no physical significance.

For materials containing impurities or solute additions, Eq.5 becomes

$$\dot{d} = \left[\frac{A}{d\Omega^{2/3}} \left(\frac{\gamma_b}{d}\right)^n \frac{\exp\left(\Delta S^*/R\right)}{C}\right] \exp\left(-Q/RT\right) \tag{6}$$

where C is the solute concentration, and A, ΔS^*, γ_b and n can vary with the magnitude of the driving force. Moreover, γ_b may vary with P depending on the atomic structure of the GB, and on the nature of the segregated solute. In the case of ceramics, the magnitude of γ_b depends on the degree and nature of the solute segregation, which in turn depends on the valence difference, as well as the size difference between the solute and solvent ions [10].

In prior work, Wang and Conrad (W-C) [16] proposed that the GB energy γ_b^0 in 3 Y-TZP consists of three major components,

$$\gamma_b^0 = \gamma_b^\Sigma + \gamma_b^s + \gamma_b^e \tag{7}$$

where γ_b^Σ results from the crystallographic misorientation between neighboring grains, γ_b^s from the ionic size difference between the yttrium ions and the solvent zirconium ions, and γ_b^e is the electrostatic space charge component, which results from the difference in valence between the segregated solute and host ions. It was determined that γ_b^e accounted for ~60% of the total GB energy γ_b^0 and the sum of the two other components about 40%. W-C [16] proposed that the reduction in γ_b^e by an externally-applied electric field was mainly responsible for the observed reduction in P and the resulting retardation in the grain growth rate in 3 Y-TZP by an electric field.

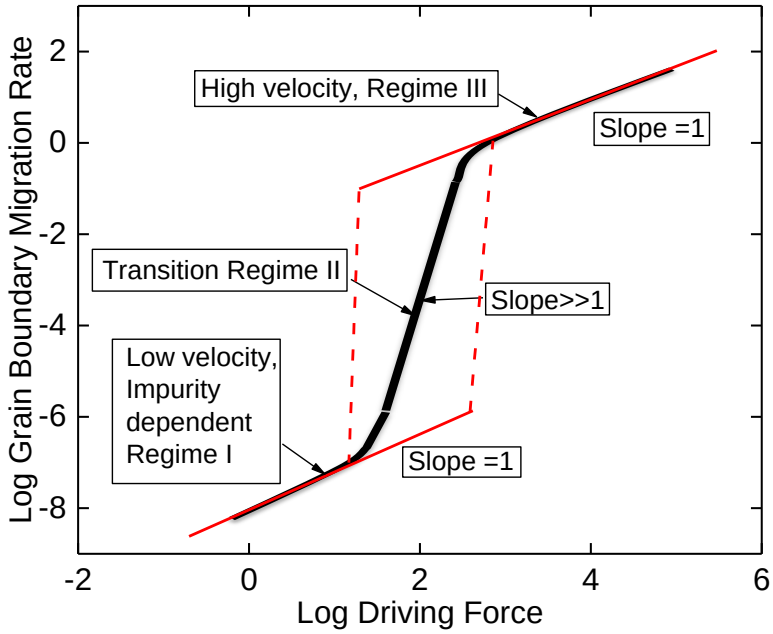

Figure 1. Schematic of log grain boundary migration rate vs log capillary driving force proposed by Vandermeer [15] for Cahn's [8] impurity drag theory.

2.2. Dynamic grain growth and concurrent cavitation

It is well-established that the plastic deformation of fine-grained materials at high homologous temperatures occurs mainly by GB sliding [4]. The observed, concurrent, dynamic grain growth in ceramics is given by [17]

$$d_d = d_0 \exp(B\epsilon) \tag{8}$$

where d_0 is the initial grain size and ϵ the overall plastic strain. The parameter B depends on the temperature T, applied strain rate $\dot{\epsilon}$ and the existing grain size d. A coupled GB sliding-migration model for dynamic grain growth in keeping with Eq.8 proposed by Wilkinson and Caceres [5] gives,

$$B = \alpha b \tag{9}$$

where $\alpha = \dot{\epsilon}_s/\dot{\epsilon}d = 0.5 - 0.8$ is the fraction of the strain rate due to the GB sliding compared to the overall strain rate $\dot{\epsilon}$. The parameter $b = cf$ represents the average migration distance per unit sliding, c being the depth of deformation zone produced per unit sliding and f is a function which depends on the GB distribution. b has a value between 3.8 and 6.

It is expected that the GB sliding which occurs during plastic deformation at high temperatures affects the governing grain growth mechanism. Clark and Alden [18] proposed that the increase in grain growth rate due to GB sliding results from an increase in the concentration of vacancies, which leads to an increase in GB mobility. However, there is no direct evidence for this. Alternatively, Grey and Higgins [19] proposed that the enhanced dynamic grain growth rate resulted from a decrease in the GB pinning due to the segregated solute clusters, or by a decrease in immobile steps in the boundary itself. They suggested that support for the latter is provided by the observation that

GB sliding and migration are observed sequential events in high purity Al, i.e. GB pinning can occur by the steps in the boundary without solute segregation.

Additional information on the mechanism for the enhanced dynamic grain growth in 3 Y-TZP is provided by the results obtained by Di Yang and Conrad (D-C) [20] in their investigation on the influence of an applied DC electric field on the two types of grain growth. These authors confirmed that the dynamic grain growth rate was greater than the static rate both without and with an applied field. Moreover, they found that the field retarded both the dynamic and static grain growth rates, but it had a greater effect on the former. This suggests that the disruption of the GB atomic structure by the GB sliding gave either an atomic arrangement at the GBs with an increase in the magnitude of the electronic component γ_b^e in the GB energy (e.g. an increase in the space charge), or gave an atomic arrangement with which the electric field had a higher degree of interaction. Di Yang and Conrad [20] further found that the amount of GB cavitation was a unique function of the grain size, independent of the applied electric field, see Figure 2.

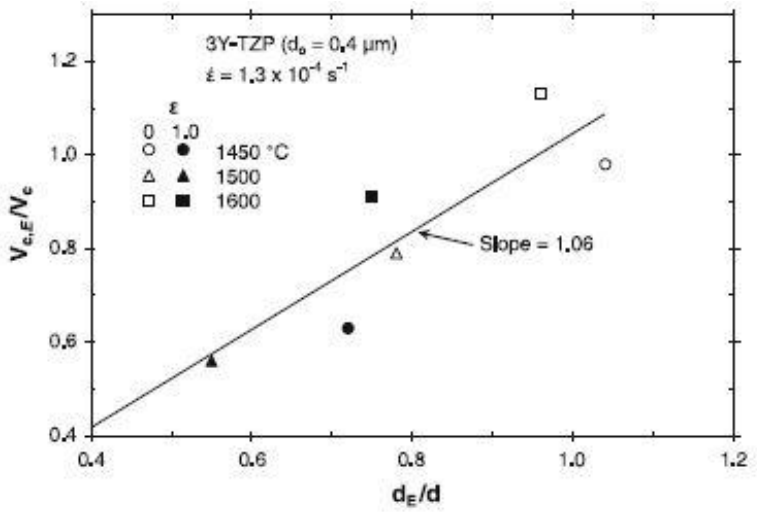

Figure 2. Cavitation ratio at the tensile plastic strains $\epsilon = 0$ and $\epsilon \approx 1.0$ for tests with and without a DC electric field vs the concurrent grain size ratio. From Di Yang and Conrad [20].

It is well-documented that concurrent with grain growth cavitation along the GBs generally occurs during the high temperature deformation of fine-grained materials [4,5,6,21]. Desirable is a knowledge of the relationship between the cavitation (which increases with plastic strain) and the existing grain size. The plastic deformation model developed by Stowell [22] gives for the effect of plastic strain ϵ on the volume fraction ϕ of cavitation voids

$$\phi = \phi_0 \exp(n\epsilon) \tag{10}$$

where ϕ_0 is the cavitation at zero strain and n is a parameter which usually has a value in the range of 2 to 3. The effect of ϵ on ϕ in 3 Y-TZP (data from Schlisser et al. [6]) is shown in Figure3. Included are measurements by Di Yang and Conrad [20] on 3 Y-TZP deformed at 1450 ℃, 1500 ℃ and 1600 ℃ with and without an applied DC electric field. The data from these two sources are in reasonable agreement, and in reasonable accord with Stowell's model [22].

Furthermore, the parameter n given by the slope of the line is relatively independent of the applied electric field. This indicates that the electrostatic component γ_b^e of the GB energy (the space charge) is not a major factor in the relationship between the cavitation ϕ and the plastic strain ϵ.

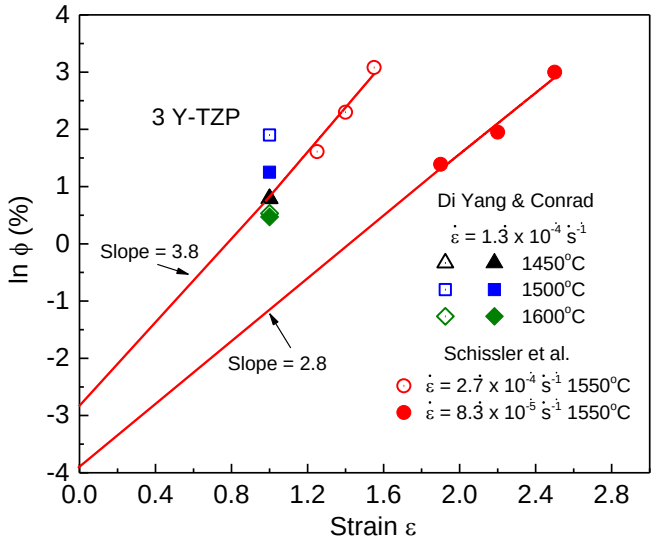

Figure 3. Natural logarithm of the amount of cavitation ϕ vs the plastic deformation strain ϵ in 3 Y-TZP. Data from Schissler et al. [6] and from Di Yang and Conrad [20]. Filled data points for tests by Di Yang and Conrad are with DC electric field. E = 10V/cm.

The model developed by Chokshi and Langdon [23] for diffusion-controlled GB cavity growth rate gives

$$\frac{dr_c}{d\epsilon} = \frac{45\Omega\delta_b D_{gb}}{d^2 kT}\left(\frac{\sigma}{\dot{\epsilon}}\right) \tag{11}$$

where r_c is the cavity radius, ϵ is the total strain, Ω is the atomic volume, δ_b is the GB width, D_{gb} is the GB diffusion coefficient and d is the grain size. According to this model the cavity growth rate *increases* appreciably with *decrease* in GS, which is in keeping with experimental results based on the *initial* grain size, but not the existing GS. As mentioned above, in general the GS increases concurrently with straining (i.e., dynamic grain growth) and this needs to be taken into account.

Although it is generally recognized that grain growth occurs concurrently with cavitation during high temperature plastic deformation, very little quantitative information is available on the relationship between cavitation and the concurrent grain growth. Considering 3 Y-TZP, it is seen in Figure 4 that there occurs an appreciable (hyperbolic) *increase* in cavitation with *increase* in grain size, contrary to the prediction by Eq.11. This gives that the observed cavitation in 3 Y-TZP is not primarily diffusion-controlled.

Figure 5 shows that the hyperbolic increase in ϕ with the concurrent increase in d_α shown in Figure 4 approximates a straight line in a plot of lnϕ vs d, which gives the empirical relationship

$$ln\phi = ln\alpha_\phi + \beta_\phi d_\alpha \tag{12}$$

where $ln\alpha_\phi \approx -2.4$ and $\beta_\phi \approx 3.4$. The value of $\alpha_\phi = 10^{-1}\%$ agrees with the relative density of fully-sintered 3Y-TZP specimens [16], and hence is the magnitude of ϕ_0. In keeping with Stowell's GB cavitation model (Eq.10), we will take $\alpha_\phi = \phi_0$ and $B_\phi d_\alpha = n\epsilon$ to give

$$ln\left(\frac{\phi}{\phi_0}\right) = n\epsilon = B_\phi d_\alpha \tag{13}$$

where $n \approx 2.5$ [22] and $B_\phi \approx 3.4$ (Fig.5), and in turn $d_\alpha = n\epsilon/B_\phi = 0.74\epsilon$. Further, Eq.13 specifies that the volume fraction of cavitation increases exponentially with the concurrent dynamic GS, in accord with the experiment. Furthermore, taking according to W-C [5] $\overline{d_\alpha} \approx \bar{x}/(0.7\epsilon)$, where $\bar{x}$ is the average GB sliding distance, and inserting for d_α in Eq.13, one obtains

$$ln\left(\frac{\phi}{\phi_0}\right) = B_\phi \bar{x}/(0.7\epsilon) \tag{13a}$$

i.e. the cavitation results from the GB sliding. Moreover, since $d_\alpha \approx \bar{x}/(0.7\epsilon)$ [5] = $n\epsilon/B_\phi$ (Eq.13), one obtains for the plastic strain dependence of $\bar{x}$

$$\bar{x} \approx \frac{0.7\epsilon n\epsilon}{B_\phi} \approx 0.51\epsilon^2 \tag{14}$$

Based on the above it is concluded that the W-C [5] coupled, sequential GB sliding-migration model is a good description of the strain dependence of the dynamic grain growth in 3Y-TZP, and moreover, the strain and grain size dependence of GB cavitation that results from the sliding.

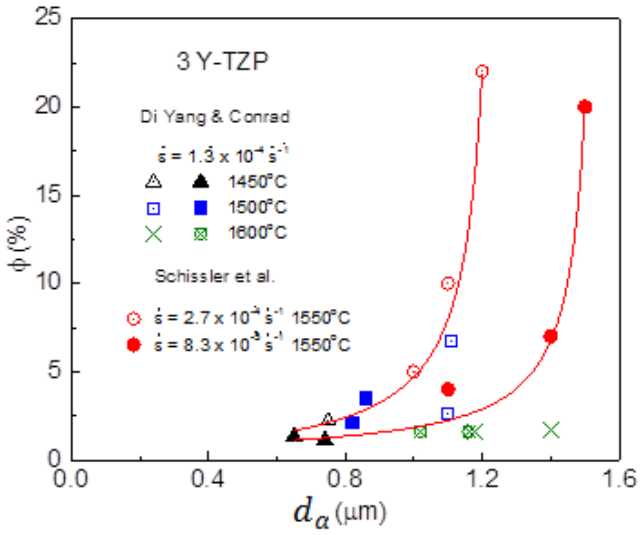

Figure 4. Amount of cavitation ϕ vs the concurrent grain size d. Data from Schissler et al. [6] and from Di Yang and Conrad [20]. Filled data points for tests by Di Yang and Conrad are with DC electric field.

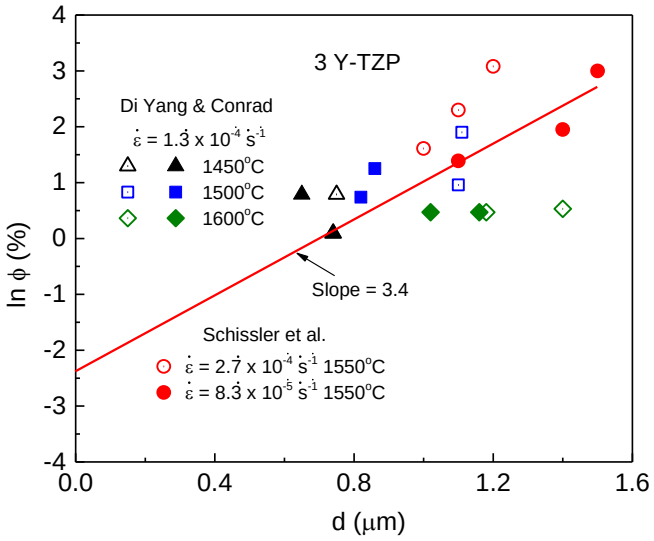

Figure 5. Natural logarithm of the amount of cavitation ϕ vs the grain size d. Data from Schissler et al. [6] and from Di Yang and Conrad [20]. Filled data points for tests by Di Yang and Conrad are with DC electric field.

3. Analysis of Data by Nieh and Wadsworth [2]

In this section we consider the data in Figures 2 and 3 in the paper by N-W [2] in terms of the models and mechanisms reviewed above. To obtain the pertinent parameters we employ the following equations:

$$d^3 - d_0^3 = K(T)t \tag{15}$$

$$d = (Kt + d_0^3)^{1/3} \tag{16}$$

$$\dot{d} = K/3d^2 \tag{17}$$

$$t = (d^3 - d_0^3)/K \tag{18}$$

$$\epsilon = \dot{\epsilon}t \tag{19}$$

where d is the mean grain size (GS), d_0 is the initial GS, K(T) is the time law constant, which is an exponential function of the temperatures, $\dot{d}$ is the grain growth rate, ϵ is the overall strain, $\dot{\epsilon}$ is the strain rate and t is the time.

Eq.6 in section 2 gives that $\dot{d}$ is proportional to $d^{-(n+1)}$, where n is the capillary driving force exponent. The magnitude of the exponent (n + 1) = p can thus be obtained from the slope of a plot of log$\dot{d}$ vs log$d$. Such slopes for the N-W data are presented in Figure6. It is seen that the results for both dynamic and static grain growth fall on straight lines with slope equal to ~2. This gives that the capillary driving force exponent n =1. The N-W data thus represents either Regime I or Regime III in Figure 1. Taking the GB energy $\gamma_b^0 = 1.215 - 0.358\ 10^{-3}T$ (J/m^2) [24], and the range of values of d in Figure 6, the magnitude of the capillary driving force in the N-W data lies in Regime I when compared with prior results [25,26]. It is therefore concluded that the N-W test results refer to Regime I.

Of further interest regarding the mechanism governing dynamic grain growth compared to static in 3 Y-TZP is the magnitudes of the activation energy Q in Eq.6 and of the pre-exponential A^* given by

$$A^* = \left(A\gamma_b/d^2\Omega^{1/3}\right)\left[\frac{\exp\left(\Delta S^*/R\right)}{C}\right] \tag{20}$$

At constant A^* (constant d^2) the magnitude of Q is given by

$$Q = Rln(\frac{\dot{d}_2}{\dot{d}_1})/(T_1^{-1} - T_2^{-1}) \tag{21}$$

where $\dot{d}_2$ and $\dot{d}_1$ are the gain growth rates, respectively, at T_1 =1550 ℃ and T_2 =1650 ℃. Having determined the values of Q, the magnitudes of A^* were obtained employing

$$A^* = (ln\dot{d})\exp\left(Q/RT\right) \tag{22}$$

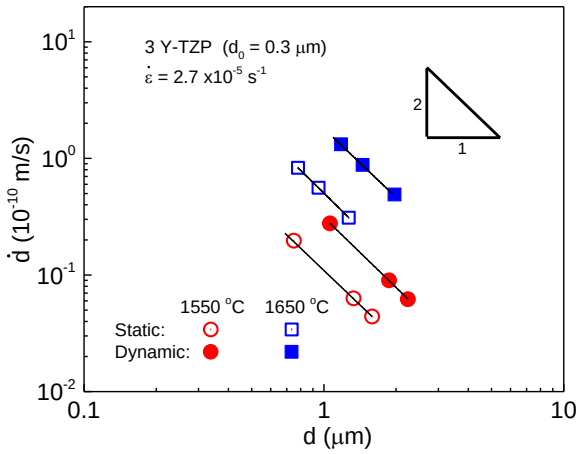

Figure 6. Log-log plot of the grain growth rate $\dot{d}$ vs the grain size d at 1550 ℃ and 1650 ℃ calculated from the data by Nich and Wadworth [2,3].

To obtain the value of $\dot{d}$ at a constant d^2 for use in Eq.21, a log-log plot of $\dot{d}$ vs d^2 is presented in Figure 7. In accord with Eq.6 the data points for both dynamic and static grain growth fall on straight lines with a slope of −1.

The values of Q and A^* as a function of the grain size d determined from the N-W data employing Eqs.21 and 22 are given in Figure 8. To be noted is that Q for both dynamic and static grain growth *increases* slightly with d, while A^* *decreases* appreciably. Both parameters are however larger for dynamic grain growth compared to static over the entire grain size range considered (e.g., Q_d = 506 kJ/mole vs Q_s = 440 kJ/mole and $logA_d^*(m/s) = 4$ vs $logA_s^*(m/s) = 2$ determined for d^2 = 1.0 $(\mu m)^2$. These larger values of Q and A^* for dynamic grain growth are in contrast to the smaller values for dynamic grain growth obtained by N-W [2] from their plots of K_d and K_s vs T^{-1}. The effect of grain size on the ratio Q_d/Q_s and the ratio A_d^*/A_s^* are shown in Figure 9. It is seen that the ratio Q_d/Q_s decreases only slightly with d, while the ratio A_d^*/A_s^* decreases appreciably.

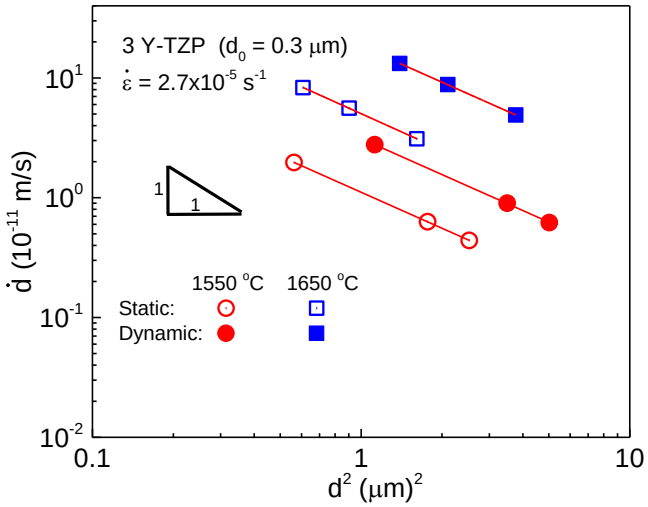

Figure 7. Log-log plot of the grain growth rate $\dot{d}$ vs. the square of the grain size d calculated from the data by Nich and Wadworth [2,3].

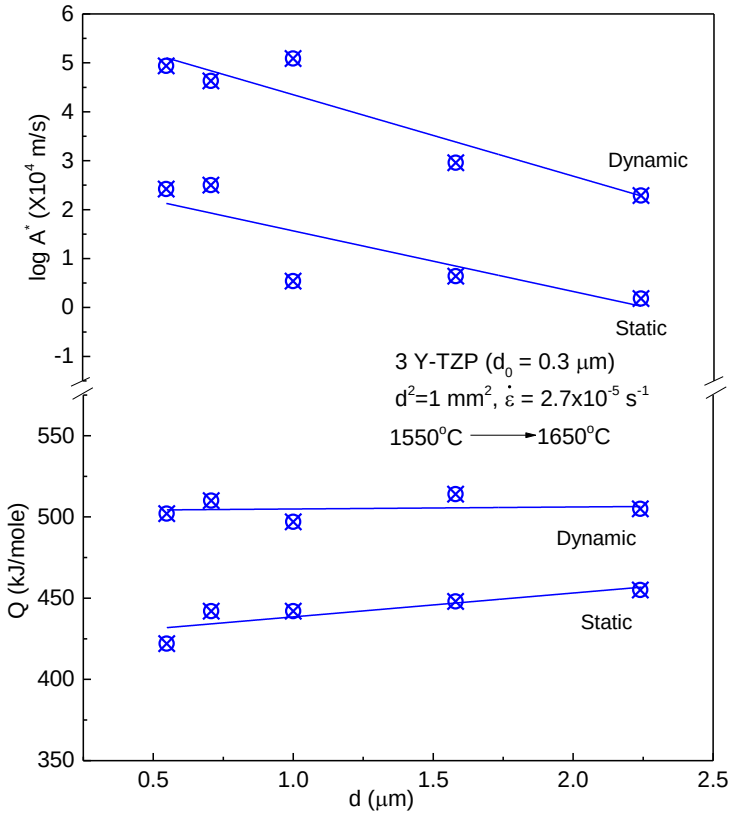

Figure 8. Variation of the static and dynamic activation energy Q and the pre-exponential A^* with grain size d for d^2 = constant at 1550 ℃ and 1650 ℃.

The results in Figs.8 and 9 thus give that the greater dynamic compared to static grain growth rate results mainly from the appreciably larger value of the pre-exponential parameter A^*. Desired is a knowledge of the parameters comprising A^* which could account for the two orders of magnitude

larger values of this factor for dynamic grain growth. Two parameters which could give a significant increase in A^* as a result of plastic deformation (GB sliding) are: (a) an increase in the number of atomic jump sites N_j due to an increase in the number of GB steps or ledges and (b) an increase in ΔS^*due to the increase in $\Delta H^* = Q$ [27] or to an otherwise disruption of the GB atomic structure [28]. Increases in the GB energy γ_b and in the atomic jump distance x^* could conceivably also contribute to the increase in A^* as a result of the disruption of the GB structure by the GB sliding.

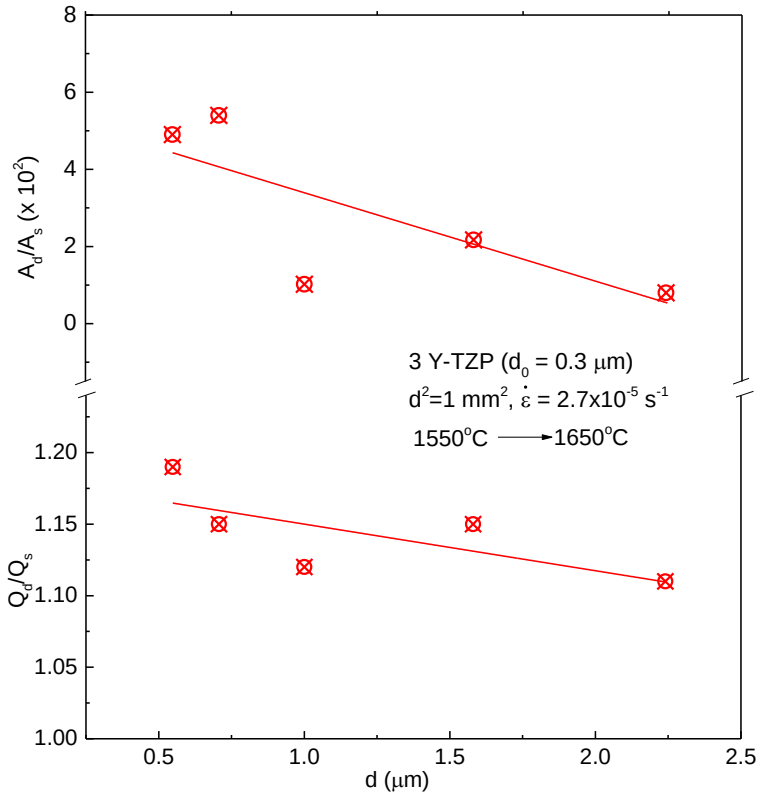

Figure 9. The variation with grain size d of the ratios $Q_{dynamic}/Q_{static}$ and $A^*_{dynamic}/A^*_{static}$ for d^2 = constant.

Regarding the effect of ΔS^* on A^*_s, the entropy of atomic migration ΔS^*_m in metals is related to the enthalpy of migration ΔH^* by [27]

$$\Delta S^*_m = \beta^*_m \Delta H^*_m / T_M \tag{23}$$

where T_M is the relating temperature and β^*_m is a constant in the range of 0.25 to 0.45 for metals, but could conceivably be higher for oxide ceramics. Taking for 3 Y-TZP, $T_M = 2837K$, $\beta^*_m = 1.0$, $\Delta H^*_{m,d} = 506$ kJ/mole and $\Delta H^*_{m,s} = 440$ kJ/mole, one obtains $\Delta S^*_{m,d} = 176$J/mole $K$and $\Delta S^*_{m,s} = 153$J/mole K. These values in turn give for the contribution of the increase in entropy to the ratio of the pre-exponential $A^*_d/A^*_s = \exp\left[\frac{\Delta S^*_{m,d} - \Delta S^*_{m,s}}{R}\right] = 15.9$, which accounts for about 1/10 of the magnitude of this ratio shown in Figs.8 and 9. The remaining order of magnitude increase must therefore result from an increase in one or more of the parameters A_{gb}, γ_b or x^* by the GB sliding. A

determination of possible increases in these parameters requires further theoretical and experimental work.

4. Conclusion

1. The overall physical mechanism governing dynamic grain growth rate is the same as that governing static grain growth.
2. An important parameter in the grain growth kinetics equation is existing grain size; i. e., the grain growth rate is proportional to d^{-2}.
3. The major factor which determines the higher dynamic compared to static grain growth rate in 3Y-TZP is the appreciably larger magnitude of the pre-exponential in the Arrhenius-type rate equation.
4. It is proposed that the slightly higher enthalpy which occurred in dynamic grain growth results from the disruption of the grain boundary atomic structure produced by the grain boundary sliding responsible for the high temperature plastic deformation.
5. A parameter which leads to the higher pre-exponential in dynamic grain growth is the increase in entropy associated with the governing atomic diffusion mechanism. It accounts for about 10% of the increase.
6. The Wilkinson-Caceres coupled, sequential grain boundary sliding-migration model provides a good description of dynamic grain growth rate.
7. The grain boundary cavitation that occurs during the plastic deformation at high temperatures increases with the concurrent grain size.
8. The grain boundary cavitation which occurred during the plastic deformation of 3Y-TZP at high temperatures resulted from the concurrent grain boundary sliding; the hyperbolic increase in cavitation which occurred with increase in grain size is due to the greater total sliding distance which occurs with a larger grain size.

Acknowledgements

The senior author Hans Conrad wishes to acknowledge prior financial support by the U.S. Army Research Office and by the Materials Science Division of the National Science Foundation. Dr. Jun Wang would like to acknowledge prior financial support by the Materials Science Division of the National Science Foundation.

Conflict of Interest

The authors declare no conflicts of interest regarding this paper.

References

1. Kingery WD, Bowen HK, Ullmann DR (1976) Introduction to Ceramics, John Wiley & Sons, New York.
2. Nieh TG, Wadsworth J (1989) Dynamic grain growth during superplastic deformation of yttria-stabilized tetragonal zirconia polycrystal. *J Am Ceram Soc* 72: 1469–1472.

3. Nieh TG, Wadsworth J (1990) Effect of grain size on superplastic behavior of Y-TZP. *Scripta Metall* 24: 763–766.
4. Sherby OD, Wadsworth J (1989) Superplasticity–recent advances and future directions. *Prog Mater Sci* 33: 169–221.
5. Wilkinson DS, Caceres CH (1984) On the mechanism of strain-enhanced grain growth during superplastic deformation. *Acta Metall* 32: 1335–1345.
6. Schissler DJ, Chokshi AH, Nieh TG, et al. (1991) Microstructural aspects of superplastic tensile deformation and cavitation in fine-grained yttria-stabilized tetragonal zirconia. *Acta Metall Mater* 39: 3227–3236.
7. Burke JE, Turnbull D (1953) Recrystallization and grain growth. *Pro Met Phys* 3: 220–292.
8. Cahn JW (1962) The impurity-drag effect in grain boundary motion. *Acta Metall* 10: 789–798.
9. Lücke K, Stüwe H-P (1963) On the theory of grain boundary motion in Recovery and Recrystallization of Metals, L. Himmel, ed., Gordon and Breach, New York, 171–210.
10. Hwang S-L, Chen I-W (1990) Grain size control of tetragonal zirconia polycrystals using the space charge concept. *J Am Ceram Soc* 73: 3269–3277.
11. Chaim R (2008) Activation energy and grain growth in polycrystalline Y-TZP ceramics. *Mater Sci Eng A* 486: 439–446.
12. Wang J, Conrad H (2015) Grain boundary curvature measurements in annealed yttria-stabilized zirconia (3Y-TZP) and their relation to mean grain size. *J Am Ceram Soc* 1–3.
13. Smith CS, Guttman L (1953) Measurement of internal boundaries in three-dimensional structures by random sectioning. *Trans AIME* 197: 81–87.
14. Wang J, Conrad H (2013) Grain boundary resistivity in yttria-stabilized zirconia. *Processing and Properties of Advanced Ceramics and Composites V: Ceramic Trans.* 240: 175–188.
15. Vandermeer RA (1967) A transient effect in grain boundary migration during recrystallization in aluminum. *Acta Metall* 156: 447–458.
16. Wang J, Conrad H (2014) Contribution of the space charge to the grain boundary energy in yttria-stabilized zirconia. *J Mater Sci* 49: 6074–6080.
17. Chen I-W, Xue LA (1990) Development of superplastic structural ceramics. *J Am Ceram Soc* 73: 2585–2609.
18. Clark MA, Alden TH (1973) Deformation enhanced grain growth in superplastic Sn-1% Bi alloy. *Acta Metall* 21: 1195–1206.
19. Grey EA, Higgins GT (1972) Solute limited grain boundary migration: A rationalisation of grain growth. *Acta Metall* 21: 309–321.
20. Yang Di, Conrad H (2008) Retardation of grain growth and cativation during superplastic deformation of ultrafine-grained 3 Y-TZP at 1450–1600 ^{o}C. *J Mater Sci* 43: 4475–4483.
21. Ma Y, Langdon TG (1994) A critical assessment of flow and cavity formation in a superplastic yttria-stabilized zirconia. *Acta Metall Mater* 42: 2753–2761.
22. Stowell RJ (1982) Cavitation in superplasticity in Superplastic Forming of Structural Alloys, N. E. Paton, C. H. Hamilton, eds., TMS, Warrendals, PA, 321–336.
23. Chokshi AH, Langdon TG (1987) A model for diffusional cavity growth in superplasticity. *Acta Metall* 15: 1089–1101.
24. Tsoga A, Nikolopoulos P (1996) Surface and grain-boundary energies in yttria-stabilized zirconia (YSZ-8 mol%). *J Mater Sci* 316: 5409–5413.

25. Wang J, Du A, Yang D, et al. (2013) Grain boundary resistivity of yttria-stabilized zirconia at 1400 ^{o}C. *J Ceram* 2013.
26. Wang J, Yang D, Conrad H (2013) Transient-regime grain growth in nanocrystalline yttria-stabilized zirconia annealed without and with a DC electric field. *Scripta Mater* 69: 351–353.
27. Shewmon PG (1963) Diffusion in Solids, McGraw-Hill, New York, 62–65.
28. Cachadiña I, Solier JD, Dominguez-Rodriguez A (1995) Activation entropy and Gibbs free energy for conduction in yttria-stabilized zirconia single crystals. *Phys Rev B* 52: 10872–10876.

AIMS Press

© 2016 Jun Wang, et al., licensee AIMS Press. This is an open access article distributed under the terms of the Creative Commons Attribution License (http://creativecommons.org/licenses/by/4.0)